Atmos. Chem. Phys. Discuss., 12, 5189–5223, 2012
www.atmos-chem-phys-discuss.net/12/5189/2012/
doi:10.5194/acpd-12-5189-2012

Atmospheric Chemistry and Physics Discussions

Model evaluation of NO_3 secondary organic aerosol (SOA) source and heterogeneous organic aerosol (OA) sink in the Western United States

J. L. Fry and K. Sackinger

Department of Chemistry, Reed College, Portland, OR, USA

Received: 15 December 2011 – Accepted: 8 February 2012 – Published: 17 February 2012

Correspondence to: J. L. Fry (fry@reed.edu)

Published by Copernicus Publications on behalf of the European Geosciences Union.

Abstract

The relative importance of NO_3-initiated source and heterogeneous sink of organic aerosol in the Western United States is investigated using the WRF/Chem regional weather and chemistry model. The model is run for the four individual months, representing the four seasons, of January, May, August, and October, to produce hourly spatial maps of surface concentrations of NO_3, organic aerosol (OA), and reactive organic gases (ROG, a sum of alkene species tracked in the lumped chemical mechanism employed). These "baseline" simulations are used in conjunction with literature data on secondary organic aerosol (SOA) mass yields, average organic aerosol composition, and reactive uptake coefficients for NO_3 on organic surfaces to predict SOA source and OA heterogeneous loss rates due to reactions initiated by NO_3. We find both source and sink rates maximized downwind of urban centers, therefore with a varying location that depends on wind direction. Both source and sink terms are maximum in summer, and SOA source dominates over OA loss by approximately three orders of magnitude, with large day-to-day variability. The NO_3 source of SOA is found to be atmospherically significant (peak production rates of 0.4–3.0 $\mu g\,kg^{-1}\,h^{-1}$), while the heterogeneous sink of OA via NO_3 surface reactions (peak loss rates of $0.11–2.3 \times 10^{-3}\,\mu g\,kg^{-1}\,h^{-1}$) is likely too small to significantly impact the atmospheric lifetime of either organic aerosol or oxidized nitrogen (NO_y).

1 Introduction

Atmospheric aerosols (liquid or solid particles suspended in air) are both an important air pollutant, with adverse visibility (Watson, 2002) and human health effects (Pope and Dockery, 2006), and a significant but poorly understood climate forcing agent (IPCC, 2007). Aerosols affect Earth's radiative balance by scattering and absorbing sunlight, and by influencing cloud formation and lifetime. The uncertainty in the overall climate forcing by aerosols arises because knowledge is incomplete on the mechanisms of

ACPD
12, 5189–5223, 2012

their production and loss. These source uncertainties are particularly large for that fraction of aerosol that is nitrate (Karydis et al., 2007; Yu et al., 2005) or organic aerosol (OA) (Hallquist et al., 2009), the latter of which comprises a substantial fraction of submicron aerosol globally (Kanakidou et al., 2005). A major fraction of OA is secondary, that is, formed by gas-to-particle conversion in the atmosphere, with source estimates varying from 50–910 TgC yr^{-1} (Hallquist et al., 2009). Higher numbers arise from top-down estimates than from bottom-up estimates, suggesting either that chamber experiments underestimate secondary organic aerosol (SOA) production from volatile organic compound (VOC) oxidation processes, or that heterogeneous aerosol loss processes are disproportionately affecting chamber experiments, relative to the real atmosphere.

One candidate for additional SOA production is the reaction of nitrate radical (NO_3) with biogenic VOCs, which comprise the majority of non-methane hydrocarbons emitted to the atmosphere (Guenther et al., 2006). Although present in low concentrations (10 s of pptv) and primarily at night, NO_3 is highly reactive with alkenes and therefore disproportionately responsible for the oxidation of biogenic VOCs, which all contain at least one double bond. Isoprene and the major monoterpenes (α-pinene, β-pinene, Δ-carene, and limonene) have a significantly shorter lifetime with respect to NO_3 than either OH or O_3, when normalized to average 24-h concentrations of each oxidant (Atkinson and Arey, 2003). SOA formation from these reactions have received sparser study, but the available experimental evidence shows substantial aerosol yields: Griffin et al. (1999) measured mass yields for $NO_3 + \Delta$-carene (13–72 %), β-pinene (32–89 %) and sabinene (14–76 %), with the large variation resulting from different initial BVOC concentrations. Hallquist et al. (1999) measured mass yield at lower BVOC concentrations of $\approx$ 10 ppb each for α-pinene (< 1 %), β-pinene (10 %), Δ-carene (15 %), and limonene (17 %). More recently, Spittler et al. (2006) measured SOA mass yield from $NO_3 + \alpha$-pinene under atmospherically relevant, seeded conditions, to be on average 10 %. Fry et al. (2009) measured the mass yield from $NO_3 + \beta$-pinene under atmospherically relevant conditions to be $\approx$ 50 %. NO_3-initiated SOA yield from isoprene

ACPD
12, 5189–5223, 2012

was recently investigated and found to be substantial: 4–24 % for 20–100 ppb of isoprene (51) or 14 % mass yield from 10 ppb isoprene, doubly nitrated (Rollins et al., 2009).

However, NO_3 radical might also act as a *sink* for OA, through heterogeneous reactions on the surface of organic particles that can result in revolatilization of some organic mass. Molina et al. (2004) demonstrated the possibility of such revolatilization in the case of OH radical, showing rapid consumption of alkane and aromatic organic monolayers, with an effective lifetime with respect to volatilization of ≈ 6 days. Laboratory studies have shown substantial uptake coefficients of NO_3 radical on organic surfaces (Moise et al., 2002; Gross et al., 2009; Gross and Bertram, 2008), and at least one recent study has focused on laboratory measurements of volatilization of an organic layer by NO_3 (Knopf et al., 2006), finding that in the case of alkanes, only 10 % of a monolayer was volatilized under the most polluted conditions. We expect this volatilization process would be more rapid with alkenes, given the 2 orders of magnitude higher uptake coefficients.

If efficient volatilization occurs, this heterogeneous reaction of NO_3 on the surface of OA may be important for atmospheric aerosol lifetimes. However, even if this is not a significant removal process for OA, it may yet be important as a loss mechanism for gas-phase NO_y. In this paper, we model the NO_3-initiated source of SOA and the sink process of NO_3 + OA, examining the latter both from the standpoint of atmospheric organic aerosol budgets and NO_y budgets.

2 Model description

For this study, the WRF/Chem model was run for four months, January, May, August, and October, using the same chemical mechanism, to capture seasonal variation in background chemistry. Surface spatial maps of nitrate radical concentration and several volatile and aerosol-phase lumped organic species are used to construct spatial maps of NO_3-initiated SOA source and maximum possible NO_3-initiated

ACPD
12, 5189–5223, 2012

consumption of OA, to assess processes governing nighttime NO_y sink, and whether NO_3 is a greater net source or sink of organic aerosol in the Western US.

2.1 WRF/Chem model runs

The fully coupled online regional chemical/dynamical Weather Research and Forecasting/Chemistry (WRF/Chem) model is employed to generate hourly spatial maps of relevant chemical species as inputs to offline calculations of SOA source and sink via nitrate radical (NO_3). WRF is a mesoscale numerical weather prediction model developed as a collaboration between federal agencies, headed by the National Center for Atmospheric Research (NCAR), designed for operational forecasting and atmospheric research (http://wrf-model.org). Meteorological initial and boundary conditions were obtained from re-analysis data available from the National Centers for Environmental Prediction (http://www.emc.ncep.noaa.gov/mmb/rreanl/). In addition to the dynamical calculations of winds, temperatures, water partitioning, etc. included in the model physics, a chemical mechanism is fully coupled at each time step (Grell et al., 2005). This adds calculation of surface emissions, including online calculation of biogenic emissions, gas phase chemistry, radiation and photolysis rates (Wild et al., 2000).

The version of the model employed here uses anthropogenic emissions at 4 km resolution from the EPA's 2005 National Emissions Inventory (http://www.epa.gov/ttnchie1/net/2005inventory.html) and calculates biogenic emissions online based on the scheme developed by Guenther and others (Grell et al., 2005; Guenther et al., 1993, 1994; Simpson et al., 1995; Schoenemeyer et al., 1997). This emissions scheme calculates emissions of isoprene, monoterpenes, and other volatile organic compounds based on USGS land use category, temperature, and radiation. These emissions are subsequently split into the chemical species available in the chosen chemical mechanism and added as a source term to the chemical processor. This disaggregation calculation also relies on land use types, splitting e.g. the monoterpene emissions differentially among internal (OLI) and terminal (OLT) olefins in the chemical mechanism depending on the land type. The Guenther module apportions the majority of monoterpene

ACPD
12, 5189–5223, 2012

emissions to the internal olefin variable (OLI) (80–98 %, depending on which of the 24 USGS land use types, e.g. grassland, coniferous or deciduous forest).

The chemical mechanism employed was the CBMZ mechanism (Zaveri and Peters, 1999), comprising 164 reactions among 67 chemical species. The aforementioned internal and terminal olefin lumped hydrocarbon species (OLI and OLT) and the individually treated isoprene (ISOP) comprise all the reactive (i.e., non-aromatic) alkenes in the gas-phase mechanism, and hence are the hydrocarbon species of interest for NO_3 gas-phase reaction. To this was added aerosol treated using the MOSAIC model (Zaveri et al., 2008) with aerosols grouped into 4 sectional bins (0.0390625–0.15625 µm, 0.15625–0.625 µm, 0.625–2.5 µm, and 2.5–10 µm), adding an additional 64 variables to describe the chemical composition (9 composition types, including organic carbon (OC)) and number/optical properties of these 4 size bins. For this study, this model was run for a domain covering the Western United States (lat: 30.3 to 49.5° N, lon: −112.30 to −126.7° W), with a horizontal resolution of 12 km by 12 km, and 26 vertical levels, non-uniformly spaced, from the surface to 110 mbar. Only the surface data is employed for further analysis.

This model was run for the months of January, May, August of 2008 and October 2004, for a domain covering the Western United States. From these month-long model runs, we extract hourly surface spatial maps of [NO_3] (ppb) and organic aerosol particulate concentration (WRF/Chem variables oc_a01, oc_a02, oc_a03, and oc_a04, in µg kg^{-1}), nighttime hours only, for the offline calculations described below.

2.2 NO_3 OA source and sink calculations

Two MATLAB programs were written to estimate aerosol formation and loss rates due to NO_3 oxidation. Both programs retrieve data from WRF output files and perform calculations in loops that repeat for each 1-h timestep and terminate according to user-specified time brackets. The results are then averaged over time and plotted by color on a map.

ACPD
12, 5189–5223, 2012

2.2.1 Modeling NO_3 SOA source

Chamber studies have determined aerosol mass yields for a variety of oxidant-VOC pairs. Table 1 shows the species and corresponding mass yields used to estimate SOA formation from NO_3, as well as rate constants for these reactions. The source program begins each loop by retrieving data from the WRF file on the concentrations of NO_3 and the selected VOCs in each geographic pixel and converting into appropriate units for the given rate constants. The reaction rates are calculated using temperature data from the WRF output for each pixel where T-dependence is available, then multiplied by the percent mass yields of the respective reactions to give an aerosol formation rate in number of reactant molecules per second. These yields are then adjusted for the masses of the original reactants to obtain mass formation rates:

$$\text{rate} = k[NO_3][VOC] \quad (1)$$

$$\text{aerosol mass formation rate} = \text{rate} \times MW_{VOC} \times \%\ \text{mass yield} \quad (2)$$

2.2.2 Modeling NO_3 OA sink

Uptake of OH is the rate-limiting step in heterogeneous OH oxidation (Molina et al., 2004). Since NO_3 has both lower uptake coefficients and lower atmospheric concentrations than OH (Gross et al., 2009), it is assumed that the rate-limiting step for NO_3 oxidation of an aerosol surface will likewise be NO_3 uptake. The reaction rate is therefore calculated using the following formula:

$$\text{rate}_{\text{uptake}} = \frac{\gamma \bar{c}(NO_3)}{4} \times \frac{SA_{OA}}{V_{\text{air}}} \times [NO_3] \quad (3)$$

where γ is the uptake coefficient on the surface of interest, $\bar{c}$ is the average molecular speed of NO_3 (calculated from temperature in each pixel and molecular weight), and $\frac{SA_{OA}}{V_{\text{air}}}$ is the surface area of organic aerosol per volume of air (defined below). An

ACPD
12, 5189–5223, 2012

uptake coefficient of 0.1 was used for unsaturated (alkene) reaction sites and 10^{-3} for saturated (alkane) sites, and the aerosol is considered to be 90 % saturated. These estimates are based on examination of the literature concerning organic aerosol composition (Alves et al., 2001; Baduel et al., 2010; Hamilton et al., 2004, 2006; Zhang et al., 2007) and NO_3 uptake coefficients on a variety of surfaces (Moise et al., 2002; Knopf et al., 2006; Gross and Bertram, 2008; Gross et al., 2009). Aromatic species were not included due to a lack of sources for uptake coefficients and an estimated low prevalence in aerosol.

The sink program begins each loop by retrieving data from the WRF file on NO_3 concentration, concentrations of organic aerosol in four size bins, temperature, and air density. Using the simplifying assumption that organic aerosol exists in discrete droplets separate from other aerosol components, the surface area of organic aerosol per volume of air is calculated based on mass concentration of organic aerosol, densities of air and organic aerosol, and average surface-area-to-volume ratios of the aerosol size bins i:

$$\frac{SA_{OA}}{V_{air}} = \sum_i \left(\frac{m_{OA}}{m_{air}}\right)_i \times \left(\frac{SA_{OA}}{V_{OA}}\right)_i \times \frac{V_{OA}}{m_{OA}} \times \frac{m_{air}}{V_{air}} \quad (4)$$

The density of organic aerosol is estimated at 2 g cm^{-3}; all other quantities are retrieved from the WRF file or determined by the simulation parameters.

The products of the reaction are determined by the oxidation mechanisms shown in Figs. 1 and 2, assuming H abstraction from saturated sites and NO_3 addition at unsaturated sites. Additional peroxide-forming reaction channels are known for alkylperoxy radicals (Calvert et al., 2000), but were not included because the products have comparatively low vapor pressures and thus do not conduce to an upper-limit estimate of volatilization. The branching ratio for the alcohol + carbonyl channel in both mechanisms is set at 0.6 (Knopf et al., 2006), while all other branches are assumed equally probable. The starting aerosol material is assumed to be 35 % aliphatic, 10 % carbonyls, 20 % alcohols, and 35 % carboxylic acids (Alves et al., 2001), and it is assumed

ACPD
12, 5189–5223, 2012

that each starting molecule has only one functional group. Where applicable, it is assumed equally likely that a functional group will become part of a radical product or a stable product. The branching ratios and aerosol composition were used to obtain a normalized statistical mixture of functional groups on nonradical products, schematically visualized in Fig. 3.

Products are assigned to the gas or condensed phase based on a 50 % volatility cutoff. According to Odum et al. (1996), gas/aerosol partitioning of organic compounds obeys the following equation:

$$\frac{[\mathrm{VOC}]_{\mathrm{aero}}}{[\mathrm{VOC}]_{\mathrm{gas}}[\mathrm{TSP}]} = \frac{760RTf_{\mathrm{OM}}}{\mathrm{MW}_{\mathrm{OM}}10^{6}\zeta P_{\mathrm{vap}}} \quad (5)$$

where [TSP] is the total suspended particulate concentration in $\mu g\,m^{-3}$, R is the ideal gas constant, $8.206 \times 10^{-5}\,m^3\,atm\,mol^{-1}\,K^{-1}$, f_{OM} is the mass fraction of absorbing organic matter in the total suspended particulates, ζ is the activity coefficient of the compound in the organic phase, $\mathrm{MW}_{\mathrm{OM}}$ is the mean molecular weight of the absorbing organic phase, and $\mathrm{P}_{\mathrm{vap}}$ is in Torr. Setting $[\mathrm{VOC}]_{\mathrm{aero}}/[\mathrm{VOC}]_{\mathrm{gas}} = 1$, we define $f_{\mathrm{OM}}[\mathrm{TSP}] = [\mathrm{OA}]$, assume $\zeta = 1$, and rearrange to give:

$$\frac{P_{\mathrm{vap}}}{[\mathrm{OA}]} = \frac{760RT}{\mathrm{MW}_{\mathrm{OM}}10^{6}} \quad (6)$$

Alves et al. (2001) found an average carbon number of 27 in organic matter extracted from aerosol in rural and urban areas of a Mediterranean climate zone. For a mean molecular weight of 400, the right-hand side of the above equation is roughly equal to $5 \times 10^{-8}\,\mathrm{Torr\,m^3\,\mu g^{-1}}$, giving the condition for 50 % volatilization:

$$\frac{P_{\mathrm{vap}}}{[\mathrm{OA}]} = 5 \times 10^{-8} \times \rho_{\mathrm{air}} \quad (7)$$

where P_{vap} is in Torr, [OA] is given in $\mu g\,kg^{-1}$ dry air, and ρ_{air} is given in $kg\,m^{-3}$.

ACPD
12, 5189–5223, 2012

Using a vapor pressure calculator based on SIMPOL (Pankow and Asher, 2008), products shown in Fig. 3 were divided by functional group composition and carbon number into bins with similar vapor pressure within the range of 2×10^{-5}–2×10^{-8} torr (the range of aerosol concentrations observed in the WRF output is about 0.2–200 µg kg^{-1} dry air). Lone carbonyl groups were modeled as ketones rather than aldehydes in this group contribution method. Products are partitioned according to this scheme, based on the ratio of the bin vapor pressure to background organic aerosol. The volatile fractions are then adjusted according to the mass of the original aerosol material and carbon number prevalence, which is modeled as a normal curve with mean 27 carbons and standard deviation 9 carbons. All vapor pressures are determined at 290 K.

3 Results and discussion

Spatial and seasonal variability in the NO_3 source and sink of aerosol can be observed in Figs. 4 and 5. The domain modeled includes the entire Western United States, encompassing Washington, Oregon, California, Nevada, and parts of Idaho and Montana. In these figures, the center map in each row shows the overall source or sink rate (µg kg^{-1} h^{-1}) of organic aerosol due to the nitrate initiated mechanisms, flanked in each case by the spatial maps of the "reagents" from which the rate was calculated. For the source calculation, the reagents are NO_3 radical and reactive organic gases (ROG), which is a sum of the surface concentrations of the reactive alkenes: isoprene (ISOP) and the lumped alkenes internal (OLI) and terminal (OLT) olefins. For the sink calculation, the reagents are NO_3 radical and organic aerosol mass concentration. Each row corresponds to a one-month average of hourly nighttime-only concentrations: January, May, August, and October.

A summary of the observed temporal variation is shown in Table 2, which compares the peak source and sink rates in the Western United States domain, calculated for the months of January, May, August, and October. The maximum in both source and sink

ACPD
12, 5189–5223, 2012

rates is in the month of August, when surface concentrations of NO_3, reactive organic gases, and organic aerosol are all at their maximum.

In the Western United States, the urban plumes of Seattle, Portland, San Francisco, and Los Angeles dominate the NO_x emissions and therefore NO_3 sources, which appear in the downwind direction, where ozone production (and thus formation of NO_3 from $NO_2 + O_3$) has maximized. For example, the Los Angeles NO_3 plume appears predominantly to the west over the Pacific Ocean in January, but predominantly to the east inland in spring, summer, and fall. Peak organic aerosol production likewise occurs over urban areas in the WRF model, resulting in a spatial pattern similarly highlighting Los Angles, Seattle, Portland, San Francisco, but also in this case Boise, Sacramento and Fresno. The reactive organic gases, in contrast, comprised dominantly of biogenic emissions, show a spatial pattern reflecting the locations of forests in the Pacific Northwest and Northern California, and a strong seasonal maximum in spring/summer.

Details of the source and sink seasonal patterns are discussed below.

3.1 Seasonal variation in predicted NO_3-initiated SOA source

Because the wintertime NO_3 plume downwind of Los Angeles falls over the Pacific Ocean, the primary NO_3-initiated SOA source region in the January simulation is likewise over the ocean, as well as being of minimum magnitude (peak = 0.4 $\mu g\,kg^{-1}\,h^{-1}$) relative to the other seasons. A smaller source of 0.10–0.15 $\mu g\,kg^{-1}\,h^{-1}$ is more widely geographically dispersed, downwind (offshore) of the San Francisco bay area, in the Sierra Nevada mountains, Las Vegas, and east of Los Angeles.

In spring (May simulation), the NO_3-initiated SOA source increases in the Sierra Nevada mountains east of San Francisco, east of Las Vegas, and a larger area east and southeast of Los Angeles, which is now downwind of these urban areas. The source rate in these regions is now in the range 0.6–0.8 $\mu g\,kg^{-1}\,h^{-1}$, with a peak of 1.2 $\mu g\,kg^{-1}\,h^{-1}$ in east Los Angeles.

In summer (August simulation), the spatial pattern is similar but most biased

ACPD
12, 5189–5223, 2012

eastward, as winds are more regularly onshore, and with larger source magnitude, especially east of Las Vegas. The Los Angeles downwind source is now in the range of 1–2 $\mu g\,kg^{-1}\,h^{-1}$, and Las Vegas peaks at 3 $\mu g\,kg^{-1}\,h^{-1}$.

In fall (October simulation), the maximum source has shifted coastward again, with wind direction once again more mixed. Peak SOA production in inner east Los Angeles is 1 $\mu g\,kg^{-1}\,h^{-1}$, with the broader regional source now of order 0.4–0.6 $\mu g\,kg^{-1}\,h^{-1}$. Hence, we see a seasonal variation of almost an order of magnitude in peak SOA source strength, from maximum in summer to minimum in winter. To put the absolute values of these source strengths in context, note that average modeled concentrations of organic aerosol range 1–4 $\mu g\,kg^{-1}$.

In all of these simulations, California SOA sources dominate and effectively wash out the smaller source terms downwind of cities in the Pacific Northwest. In Sect. 3.5 below, we will examine a few days of simulation exclusively in this region, to interpret the spatial and temporal variability of this smaller but nevertheless regionally significant SOA source.

3.2 Seasonal variation in predicted NO_3 OA sink

Because the organic aerosol peak concentrations are more localized to urban areas than reactive organic gases, the NO_3-initiated OA sink rates are more localized than the corresponding source terms. Still, the peaks appear downwind of urban areas where NO_3 radical concentrations are maximized. Because the peak source and sink terms are co-located with the peak [NO_3], the ratio of these peak concentrations provides a useful metric of the relative importance of NO_3 as a source and sink of organic aerosol. As shown in Table 2, the predicted SOA source from NO_3 is three orders of magnitude larger than the NO_3-initiated sink throughout the year. Peak revolatilization rates range from 1.1×10^{-4} $\mu g\,kg^{-1}\,h^{-1}$ offshore west of Los Angeles in January to 2.3×10^{-3} $\mu g\,kg^{-1}\,h^{-1}$ northeast of Los Angeles in August, with highly spatially "focused" spatial patterns, with the exception of October, when the overlap between NO_3 and OA plumes is minimal, such that regional elevated revolatilization rates of

ACPD
12, 5189–5223, 2012

1.5×10^{-4} μg kg^{-1} h^{-1} are visible in comparison with the downwind of LA peak.

What is the consequence of these rates of revolatilization for OA atmospheric lifetime? For the August Los Angeles peak OA concentration of 4 μg kg^{-1} and peak loss rate of 2.3×10^{-3} μg kg^{-1} h^{-1}, the effective organic aerosol lifetime is:

$$\tau_{OA} = \frac{[OA]}{\text{Loss rate of OA}} \quad (8)$$

giving a lifetime of 1700 h, or 70 days. For comparison, the estimate of OA lifetime with respect to OH revolatilization was ≈ 6 days (Molina et al., 2004).

3.3 Sensitivity tests

The variability of aerosol formation predicted by the aerosol source program was tested by setting all aerosol yields first to 5 % and then to 95 %. The change in aerosol formation is linearly proportional to the mass yields used.

The variability of the volatilization predicted by the aerosol sink program was tested through several modifications: assuming 100 % unsaturated aerosol, setting a carbon number distribution with mean 15 and standard deviation 5, assuming 97 % aliphatic aerosol, and assuming all bond scission products to be volatile (Table 3). Altering the unsaturated content of the aerosol increased volatilization by approximately one order of magnitude; all of the other tests produced changes of less than one order of magnitude. Changes in vapor pressures linked to temperature are another possible source of variation not captured by the model. The calculated vapor pressure of a representative product molecule (27 carbons, 1 nitrate, 1 ketone) changes by approximately one order of magnitude between 285 and 295 K, while differences between vapor pressure bins are about 1.5 orders of magnitude. However, using a carbon number distribution centered at 15 is equivalent to shifting all products by about four vapor pressure bins; thus, the impact of temperature variation is expected to be less than that represented by the carbon number sensitivity test.

ACPD
12, 5189–5223, 2012

3.4 Effect of heterogeneous NO_3 loss on nighttime NO_y budget

The above analysis, showing modeled OA sink rates several orders of magnitude lower than the corresponding source terms, even at the extremes of sensitivity testing, suggests that atmospheric NO_3 is much more important for aerosol production than its heterogeneous revolatilization. Still, this heterogeneous uptake on the surface of existing organic aerosol may be important for the nighttime budget of oxidized nitrogen species (NO_y) by providing a loss term for NO_3. To assess the importance of this process, we plot the loss rate of NO_3 in ppt h^{-1} in Fig. 6. Again, the peak importance of this process occurs downwind of Los Angeles, with a maximum loss rate of 1.4 ppt h^{-1} in August. This corresponds to an August minimum in nitrate lifetime, calculated analogously to the OA lifetime in Eq. (8), of 50 ppt/1.4 ppt h^{-1} = 36 h. Because NO_3 is photolyzed rapidly every sunrise, this loss process does not significantly limit the lifetime of NO_3 radical throughout most of the troposphere. In any region where alkenes are present, NO_3 homogeneous reaction will be more important than heterogeneous reaction: NO_3 reactivity is much higher with gas-phase alkenes. For example, the NO_3 lifetime with respect to reaction with α-pinene present at a typical concentration of 100 ppt would be 70 s ($k_{NO_3+apin} = 6 \times 10^{-12}$ cm^3 $molec^{-1}$ s^{-1}, Calvert et al., 2000).

3.5 Night-to-night variability in spatial patterns

Because meteorology and emissions vary day-to-day, the monthly averaged results necessarily present dampened maxima relative to individual nightly data, which have varying peak intensity and location. Several individual nightly averages are shown in Figs. 7–10 to illustrate this variability. We also plot several individual nights' maps for source and sink rates zoomed in on only the Pacific Northwest, to highlight spatial and temporal variability, as well as the overall magnitudes of these processes without the washing-out effect of including the California cities on the same z-axis.

In the SOA source maps (Figs. 7 and 8), most nightly maxima are significantly higher

ACPD
12, 5189–5223, 2012

(up to a factor of three) than the monthly average, with large spatial variation in peak location primarily responsible for the monthly averages being lower. For example, Fig. 7 shows a day (12. August) when Las Vegas' plume dominates the entire west coast domain, three days when the San Francisco/Sacramento plume competes with that of Los Angeles (14–16 August), two days when Seattle competes (16–17 August), as well as the large night-to-night variation in the shape of the Los Angeles source plume.

In the OA sink maps (Figs. 9 and 10), less spatial variation is obvious, suggesting that the location of organic aerosol plume is more constant than reactive organic gases. There is more variability in magnitude than spatial patterns, with an apparently wider distribution around the monthly average than in the source model.

In both source and sink maps, more spatial variation is apparent in the (overall lower) rates for the smaller Pacific Northwest domain (Figs. 8 and 10). In these zoomed maps, the occasionally significant NO_3 SOA source rates for the Portland metropolitan area, Spokane, WA, and Boise, ID are apparent. There is a region of higher organic aerosol in Southeastern Washington which occasionally overlaps a large NO_x plume from the Boardman coal-fired power plant along the Columbia River in Boardman, OR, giving sporadically larger OA loss rates in that region. Boise's urban plume dominates on other days.

3.6 Atmospheric relevance

To put these results into context, we seek to compare the NO_3-initiated OA production rates determined here to other studies of SOA sources. Results available from global and regional studies are often reported in terms of surface OA concentrations from various formation mechanisms (Robinson et al., 2007; Pye et al., 2010) or in terms of total global sources in $TgC\,yr^{-1}$ (Hallquist et al., 2009).

Two recent studies of SOA production mechanisms have reported peak surface concentrations of organic aerosol of up to $4\,\mu g\,m^{-3}$ over urban areas in the Eastern US from "traditional" SOA precursors (Robinson et al., 2007), and up to $3.35\,\mu g\,m^{-3}$ over the US from NO_3 + monoterpenes and isoprene in August (Pye et al., 2010). These

ACPD
12, 5189–5223, 2012

numbers can be qualitatively compared to the OA source rate determined here by assuming an aerosol lifetime and steady-state concentration. Our results suggest a peak SOA source of 3 $\mu g\,kg^{-1}\,h^{-1}$ and more representative regionally distributed source of order 0.2–0.4 $\mu g\,kg^{-1}\,h^{-1}$ for the month of August. These regional numbers can be converted to increases in surface OA concentration in $\mu g\,m^{-3}$ using the density of dry air (1.2 $kg\,m^{-3}$) and an estimated OA lifetime, using equation 8. The lifetime of organic aerosol has been estimated to be 4 days (Liousse et al., 1996), assuming wet deposition to be the dominant sink. This gives regional SOA source rates of 0.24–0.48 $\mu g\,m^{-3}\,h^{-1}$, which would correspond to increases in OA concentration of 23–46 $\mu g\,m^{-3}$ at peak nighttime production in areas where this NO_3-initiated SOA chemistry is important (aqua and "hotter" colored regions in Fig. 4). This large additional source estimate, an order of magnitude larger than Pye et al.'s NO_3 + monoterpene and Robinson et al.'s traditional SOA estimates, suggests that this crude lifetime analysis overestimates this source, but nevertheless that this mechanism is likely to be significant regionally.

An alternative method of comparison is to calculate for our model domain the total additional OA source predicted in TgC yr^{-1} and compare to global estimates of SOA source. Global estimates of anthropogenic SOA and biogenic SOA are 2–12 Tg yr^{-1} (Henze et al., 2008) and 13–70 Tg yr^{-1} (Kanakidou et al., 2005), respectively. These numbers refer to total organic aerosol mass, assuming a ratio of 1.4 organic matter to organic carbon. In our model for the month of August, summed averaged surface OA source from NO_3 + reactive organic gases in the Western US domain is 1.4 Tg yr^{-1} (average nighttime production rate of 0.0894 $\mu g\,m^{-3}\,h^{-1}$ over a domain area of 2.3×10^{15} m^2, with mean lowest layer height of 790 m).

Both of these model-derived source estimates are necessarily overestimates, because this offline calculation does not consume NO_3 radical, ROG, or OA in the model at each time step. However, our model results clearly demonstrate that the source greatly exceeds any heterogeneous sink initiated by NO_3. Furthermore, the large magnitude of the predicted SOA source relative to global estimates suggests that this

ACPD
12, 5189–5223, 2012

process should be included online in models, as it is likely to be significant both in terms of OA production and as a NO_3 radical sink.

4 Conclusions

NO_3 radical-initiated chemistry is predicted to be significantly more important as a *source* of organic aerosol than as a heterogeneous *sink* of organic aerosol in the Western United States. However, significant spatial and day-to-day variability in modeled source and sink suggest that both processes are important in certain locations at some times, in particular, downwind of urban areas on summer nights when terpene emissions have been large. Comparison of the average modeled NO_3 + alkene source for the Western United States to other regional and global predictions of total organic aerosol loading suggests that this process is likely an important contributor to both OA and nitrate radical budgets.

Supplementary material related to this article is available online at: http://www.atmos-chem-phys-discuss.net/12/5189/2012/acpd-12-5189-2012-supplement.pdf.

Acknowledgements. The WRF/Chem model runs were performed using EMSL (project # 30394), a national scientific user facility sponsored by the Department of Energy's Office of Biological and Environmental Research and located at Pacific Northwest National Laboratory. The authors gratefully acknowledge helpful discussions with Jerome Fast (PNNL) while setting up the model.

ACPD
12, 5189–5223, 2012

References

Alves, C., Pio, C., and Duarte, A.: Composition of extractable organic matter of air particles from rural and urban Portuguese area, Atmos. Environ., 35, 5485–5496, 2001. 5196, 5197

Atkinson, R. and Arey, J.: Gas-phase tropospheric chemistry of biogenic volatile organic compounds: a review, Atmos. Environ., 37, Supplement 2, 197–219, doi:10.1016/S1352-2310(03)00391-1, available at: http://www.sciencedirect.com/science/article/pii/S1352231003003911, 2003. 5191

Baduel, C., Voisin, D., and Jaffrezo, J.-L.: Seasonal variations of concentrations and optical properties of water soluble HULIS collected in urban environments, Atmos. Chem. Phys., 10, 4085–4095, doi:10.5194/acp-10-4085-2010, 2010. 5196

Calvert, J., Atkinson, J., Kerr, J., Madronich, S., Moortgat, G. K., Wallington, T., and Yarwood, G.: Mechanisms of the Atmospheric Oxidation of the Alkenes, Oxford University Press, New York, NY, 2000. 5196, 5202, 5211

Fry, J. L., Kiendler-Scharr, A., Rollins, A. W., Wooldridge, P. J., Brown, S. S., Fuchs, H., Dubé, W., Mensah, A., dal Maso, M., Tillmann, R., Dorn, H.-P., Brauers, T., and Cohen, R. C.: Organic nitrate and secondary organic aerosol yield from NO_3 oxidation of β-pinene evaluated using a gas-phase kinetics/aerosol partitioning model, Atmos. Chem. Phys., 9, 1431–1449, doi:10.5194/acp-9-1431-2009, 2009. 5191, 5211

Grell, G. A., Peckham, S. E., Schmitz, R., McKeen, S. A., Frost, G., Skamarock, W. C., and Eder, B.: Fully coupled online chemistry within the WRF model, Atmos. Environ., 39, 6957–6975, doi:10.1016/j.atmosenv.2005.04.027, available at: http://www.sciencedirect.com/science/article/pii/S1352231005003560, 2005. 5193

Griffin, R. J., Flagan, R. C., and Seinfeld, J. H.: Organic aerosol formation from the oxidation of biogenic hydrocarbons, J. Geophys. Res., 104, 3555–3568, doi:10.1029/1998JD100049, 1999. 5191

Gross, S. and Bertram, A. K.: Reactive uptake of NO_3, N_2O_5, NO_2, HNO_3, and O_3 on three types of polycyclic aromatic hydrocarbon surfaces, J. Phys. Chem. A, 112, 3104–3113, doi:10.1021/jp7107544, available at: http://pubs.acs.org/doi/abs/10.1021/jp7107544, pMID:18311955, 2008. 5192, 5196

Gross, S., Iannone, R., Xiao, S., and Bertram, A. K.: Reactive uptake studies of NO_3 and N_2O_5 on alkenoic acid, alkanoate, and polyalcohol substrates to probe nighttime aerosol chemistry, Phys. Chem. Chem. Phys., 11, 7792–7803, doi:10.1039/B904741G, available at:

ACPD
12, 5189–5223, 2012

http://dx.doi.org/10.1039/B904741G, 2009. 5192, 5195, 5196
Guenther, A., Zimmerman, P., Harley, P., Monson, R., and Fall, R.: Isoprene and monoterpene emission rate variability: model evaluations and sensitivity analyses, J. Geophys. Res., 98, 12609–12617, 1993. 5193
Guenther, A., Zimmerman, P., and Wildermuth, M.: Natural volatile organic compound emission rate estimates for U.S. woodland landscapes, Atmos. Environ., 28, 1197–1210, doi:10.1016/1352-2310(94)90297-6, 1994. 5193
Guenther, A., Karl, T., Harley, P., Wiedinmyer, C., Palmer, P. I., and Geron, C.: Estimates of global terrestrial isoprene emissions using MEGAN (Model of Emissions of Gases and Aerosols from Nature), Atmos. Chem. Phys., 6, 3181–3210, doi:10.5194/acp-6-3181-2006, 2006. 5191
Hallquist, M., Wangberg, I., Ljungstrom, E., Barnes, I., and Becker, K. H.: Aerosol and product yields from NO_3 radical-initiated oxidation of selected monoterpenes, Environ. Sci. Technol., 33, 553–559, 1999. 5191
Hallquist, M., Wenger, J. C., Baltensperger, U., Rudich, Y., Simpson, D., Claeys, M., Dommen, J., Donahue, N. M., George, C., Goldstein, A. H., Hamilton, J. F., Herrmann, H., Hoffmann, T., Iinuma, Y., Jang, M., Jenkin, M. E., Jimenez, J. L., Kiendler-Scharr, A., Maenhaut, W., McFiggans, G., Mentel, Th. F., Monod, A., Prévôt, A. S. H., Seinfeld, J. H., Surratt, J. D., Szmigielski, R., and Wildt, J.: The formation, properties and impact of secondary organic aerosol: current and emerging issues, Atmos. Chem. Phys., 9, 5155–5236, doi:10.5194/acp-9-5155-2009, 2009. 5191, 5203
Hamilton, J. F., Webb, P. J., Lewis, A. C., Hopkins, J. R., Smith, S., and Davy, P.: Partially oxidised organic components in urban aerosol using GCXGC-TOF/MS, Atmos. Chem. Phys., 4, 1279–1290, doi:10.5194/acp-4-1279-2004, 2004. 5196
Hamilton, J. F., Lewis, A. C., Reynolds, J. C., Carpenter, L. J., and Lubben, A.: Investigating the composition of organic aerosol resulting from cyclohexene ozonolysis: low molecular weight and heterogeneous reaction products, Atmos. Chem. Phys., 6, 4973–4984, doi:10.5194/acp-6-4973-2006, 2006. 5196
Henze, D. K., Seinfeld, J. H., Ng, N. L., Kroll, J. H., Fu, T.-M., Jacob, D. J., and Heald, C. L.: Global modeling of secondary organic aerosol formation from aromatic hydrocarbons: high-vs. low-yield pathways, Atmos. Chem. Phys., 8, 2405–2420, doi:10.5194/acp-8-2405-2008, 2008. 5204
IPCC: Climate Change 2007 – The Physical Science Basis: Working Group I Contribution to

ACPD
12, 5189–5223, 2012

the Fourth Assessment Report of the IPCC, Cambridge University Press, Cambridge, UK and New York, NY, USA, http://www.ipcc.ch, 2007. 5190

Kanakidou, M., Seinfeld, J. H., Pandis, S. N., Barnes, I., Dentener, F. J., Facchini, M. C., Van Dingenen, R., Ervens, B., Nenes, A., Nielsen, C. J., Swietlicki, E., Putaud, J. P., Balkanski, Y., Fuzzi, S., Horth, J., Moortgat, G. K., Winterhalter, R., Myhre, C. E. L., Tsigaridis, K., Vignati, E., Stephanou, E. G., and Wilson, J.: Organic aerosol and global climate modelling: a review, Atmos. Chem. Phys., 5, 1053–1123, doi:10.5194/acp-5-1053-2005, 2005. 5191, 5204

Karydis, V. A., Tsimpidi, A. P., and Pandis, S. N.: Evaluation of a three-dimensional chemical transport model (PMCAMx) in the Eastern United States for all four seasons, J. Geophys. Res.-Atmos., 112, D14211, doi:10.1029/2006JD007890, 2007. 5191

Knopf, D., Mak, J., Gross, S., and Bertram, A.: Does atmospheric processing of saturated hydrocarbon surfaces by NO_3 lead to volatilization?, Geophys. Res. Lett., 33, L17816, doi:10.1029/2006GL026884, 2006. 5192, 5196

Liousse, C., Penner, J. E., Chuang, C., Walton, J. J., Eddleman, H., and Cachier, H.: A global three-dimensional model study of carbonaceous aerosols, J. Geophys. Res., 107, 19411–19432, doi:10.1029/95JD03426, 1996. 5204

Moise, T., Talukdar, R. K., Frost, G. J., Fox, R. W., and Rudich, Y.: Reactive uptake of NO_3 by liquid and frozen organics, J. Geophys. Res., 101, doi:10.1029/2001JD000334, 2002. 5192, 5196

Molina, M. J., Ivanov, A. V., Trakhtenberg, S., and Molina, L. T.: Atmospheric evolution of organic aerosol, Geophys. Res. Lett., 312, L22104, doi:10.1029/2004GL020910, 2004. 5192, 5195, 5201

Odum, J. R., Hoffmann, T., Bowman, F., Collins, D., Flagan, R. C., and Seinfeld, J. H.: Gas/partitioning and secondary organic aerosol yields, Environ. Sci. Technol., 30, 2580–2585, 1996. 5197

Pankow, J. F. and Asher, W. E.: SIMPOL.1: a simple group contribution method for predicting vapor pressures and enthalpies of vaporization of multifunctional organic compounds, Atmos. Chem. Phys., 8, 2773–2796, doi:10.5194/acp-8-2773-2008, 2008. 5198

Pope, C. and Dockery, D.: Critical review: health effects of fine particulate air pollution: lines that connect, J. Air Waste Manage., 6, 709–742, 2006. 5190

Pye, H. O. T., Chan, A. W. H., Barkley, M. P., and Seinfeld, J. H.: Global modeling of organic aerosol: the importance of reactive nitrogen (NO_x and NO_3), Atmos. Chem. Phys., 10,

ACPD
12, 5189–5223, 2012

11261–11276, doi:10.5194/acp-10-11261-2010, 2010. 5203
Robinson, A. L., Donahue, N. M., Shrivastava, M. K., Weitkamp, E. A., Sage, A. M., Grieshop, A. P., Lane, T. E., Pierce, J. R., and Pandis, S. N.: Rethinking organic aerosols: semivolatile emissions and photochemical aging, Science, 315, 1259–1262, doi:10.1126/science.1133061, available at: http://www.sciencemag.org/content/315/5816/1259.abstract, 2007. 5203
Rollins, A. W., Kiendler-Scharr, A., Fry, J. L., Brauers, T., Brown, S. S., Dorn, H.-P., Dubé, W. P., Fuchs, H., Mensah, A., Mentel, T. F., Rohrer, F., Tillmann, R., Wegener, R., Wooldridge, P. J., and Cohen, R. C.: Isoprene oxidation by nitrate radical: alkyl nitrate and secondary organic aerosol yields, Atmos. Chem. Phys., 9, 6685–6703, doi:10.5194/acp-9-6685-2009, 2009. 5192, 5211
Schoenemeyer, T., Richter, K., and Smiatek, G.: Vorstudie über ein räumlich und zeitlich aufgelöstes Kataster anthropogener und biogener Emissionen für Bayern mit Entwicklung eines Prototyps und Anwendung fur Immissionsprognosen: Abschlussbericht an das Bayerische Landesamt für Umweltschutz, Tech. rep., Fraunhofer-Institut für Atmosphärische Umweltforschung, Garmisch-Partenkirchen, 1997. 5193
Simpson, D., Guenther, A., Hewitt, C. N., and Steinbrecher, R.: Biogenic emissions in Europe 1. Estimates and uncertainties, J. Geophys. Res., 100, 22875–22890, doi:10.1029/95JD02368, 1995. 5193
Spittler, M., Barnes, I., Bejan, I., Brockmann, K. J., Benter, T., and Wirtz, K.: Reactions of NO_3 radicals with limonene and alpha-pinene: product and SOA formation, Atmos. Environ., 40, S116–S127, doi:10.1016/j.atmosenv.2005.09.093, 2006. 5191, 5211
Watson, J.: Critical Review – visibility: science and regulation, J. Air Waste Manage., 52, 628–713, 2002. 5190
Wild, O., Zhu, X., and Prather, M.: Fast-J: Accurate simulation of in- and below-cloud photolysis in tropospheric chemical models, J. Atmos. Chem., 37, 245–282, doi:10.1023/A:1006415919030, available at: http://dx.doi.org/10.1023/A:1006415919030, 2000. 5193
Yu, S., Dennis, R., Roselle, S., Nenes, A., Walker, J., Eder, B., Schere, K., Swall, J., and Robarge, W.: An assessment of the ability of three-dimensional air quality models with current thermodynamic equilibrium models to predict aerosol NO_3^-, J. Geophys. Res.-Atmos., 110, D07S13, doi:10.1029/2004JD004718, 2005. 5191
Zaveri, R. A. and Peters, L. K.: A new lumped structure photochemical mechanism for large-

ACPD
12, 5189–5223, 2012

scale applications, J. Geophys. Res., 1043, 30387–30416, doi:10.1029/1999JD900876, 1999. 5194

Zaveri, R. A., Easter, R. C., Fast, J. D., and Peters, L. K.: Model for Simulating Aerosol Interactions and Chemistry (MOSAIC), J. Geophys. Res., 113, doi:10.1029/2007JD008782, 2008. 5194

Zhang, Q., Jimenez, J. L., Canagaratna, M. R., Allan, J. D., Coe, H., Ulbrich, I., Alfarra, M. R., Takami, A., Middlebrook, A. M., Sun, Y. L., Dzepina, K., Dunlea, E., Docherty, K., DeCarlo, P. F., Salcedo, D., Onasch, T., Jayne, J. T., Miyoshi, T., Shimono, A., Hatakeyama, S., Takegawa, N., Kondo, Y., Schneider, J., Drewnick, F., Borrmann, S., Weimer, S., Demerjian, K., Williams, P., Bower, K., Bahreini, R., Cottrell, L., Griffin, R. J., Rautiainen, J., Sun, J. Y., Zhang, Y. M., and Worsnop, D. R.: Ubiquity and dominance of oxygenated species in organic aerosols in anthropogenically-influenced Northern Hemisphere midlatitudes, Geophys. Res. Lett., 34, doi:10.1029/2007GL029979, 2007.

5196

ACPD

12, 5189–5223, 2012

Table 1. Literature SOA mass yields from NO_3 oxidation used in this model.

WRF/Chem species	Proxy	Mass yield	Rate constant (k), $cm^3\ molec^{-1}\ s^{-1}$
Isoprene (ISOP)	isoprene	14 % (Rollins et al., 2009)	$(3.03 \times 10^{-12})\ e^{-446\ K/T}$ (Calvert et al., 2000)
Internal olefin (OLI)	α-pinene	10 % (Spittler et al., 2006)	$(1.19 \times 10^{-12})\ e^{490\ K/T}$ (Calvert et al., 2000)
Terminal olefin (OLT)	β-pinene	50 % (Fry et al., 2009)	(2.41×10^{-12}) at 290 K (Calvert et al., 2000)

ACPD
12, 5189–5223, 2012

Table 2. Summary of of peak rates of NO_3 initiated production and loss of aerosol over four seasons.

Month	Maximum OA sink rate ($\mu g\,kg^{-1}\,h^{-1}$)	Maximum OA source rate ($\mu g\,kg^{-1}\,h^{-1}$)	$\frac{\text{Source}}{\text{Sink}}$
Jan	1.1×10^{-4}	0.4	3600
May	8.0×10^{-4}	1.2	1500
Aug	2.3×10^{-3}	3.0	1300
Oct	4.9×10^{-4}	1.1	2200

ACPD
12, 5189–5223, 2012

Table 3. Results of model sensitivity tests.

Modification	Maximum Jan aerosol loss rate (L.A. plume, $\mu g\,kg^{-1}\,h^{-1}$)	Maximum Jan aerosol formation rate (L.A. plume, $\mu g\,kg^{-1}\,h^{-1}$)
Unmodified source	–	0.4
All mass yield 5 %	–	0.06
All mass yield 95 %	–	1.1
Unmodified sink	1.3×10^{-4}	–
100 % unsaturated aerosol	1.2×10^{-3}	–
Carbon number mean = 15	2.5×10^{-4}	–
97 % aliphatic aerosol	1.8×10^{-4}	–
All bond scission products volatile	1.4×10^{-4}	–

ACPD
12, 5189–5223, 2012

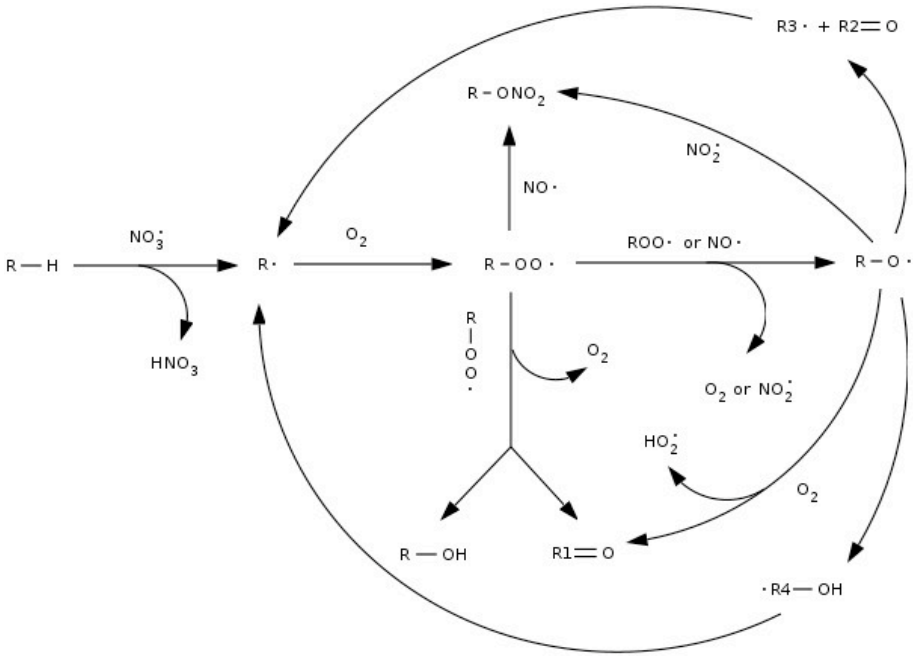

Fig. 1. Mechanism for NO_3 oxidation of an alkane.

ACPD
12, 5189–5223, 2012

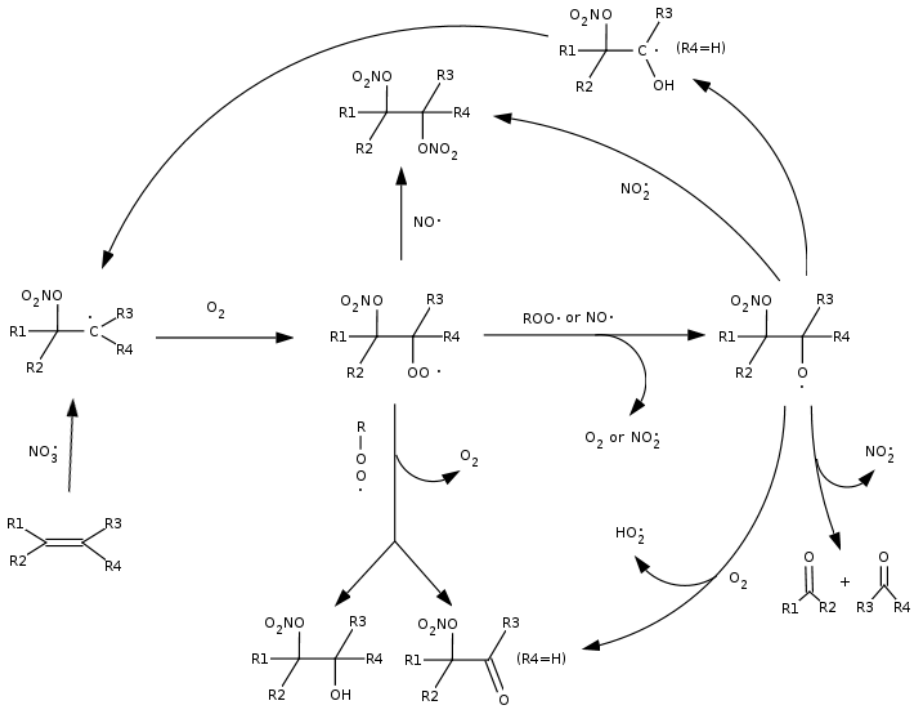

Fig. 2. Mechanism for NO_3 oxidation of an alkene.

ACPD
12, 5189–5223, 2012

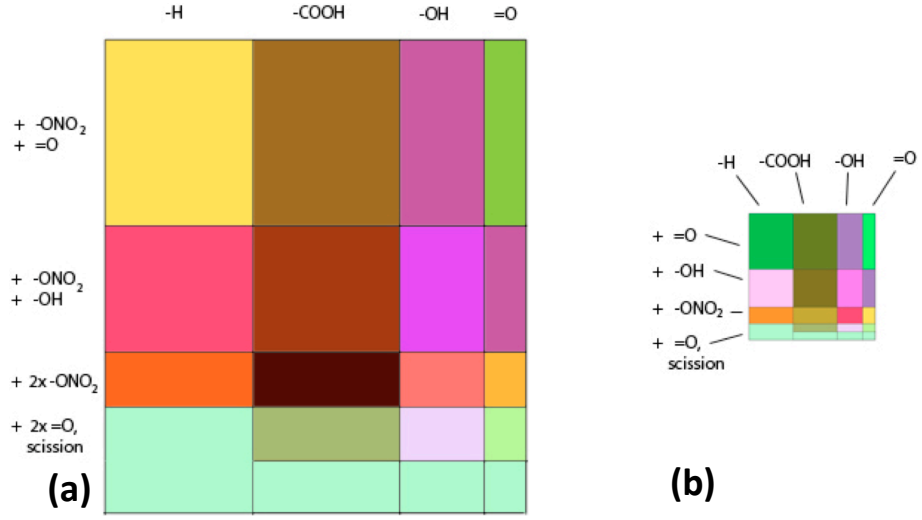

Fig. 3. Schematic of the mass-percent-weighted amount of each initial aerosol functional group component (across top), showing the percent-weighted amount which undergoes each type of reaction (along left side), for **(a)** alkene and **(b)** alkane reaction pathways. The smaller size of the alkane product matrix represents its overall lower contribution to the products: although 90 % of initial aerosol is saturated, reactions rates are much higher with unsaturated organics.

ACPD
12, 5189–5223, 2012

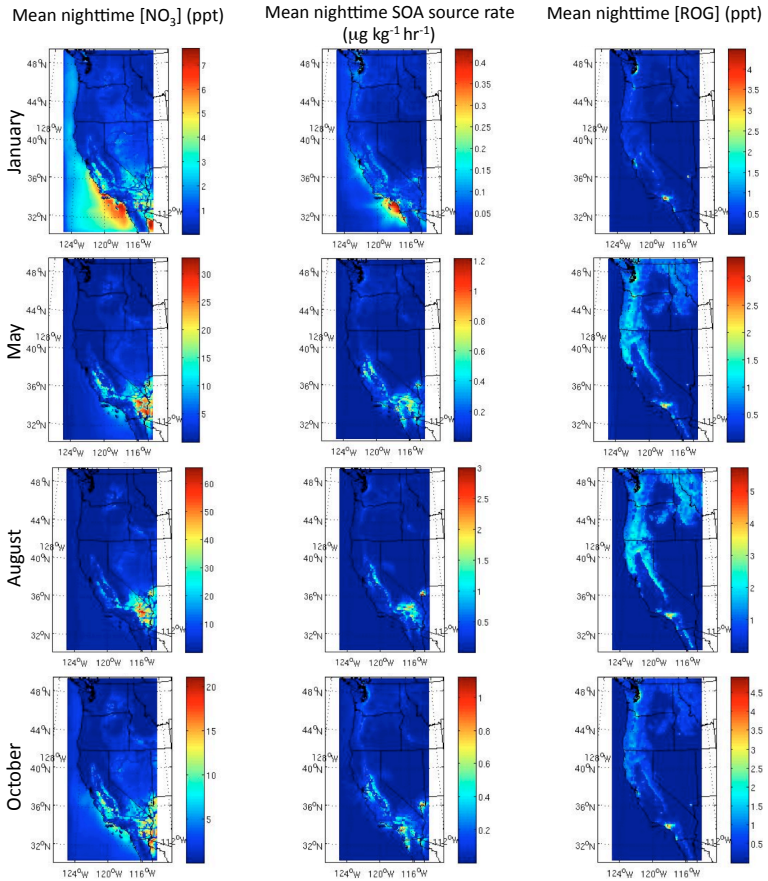

Fig. 4. Seasonal pattern of NO_3-initiated SOA source rate (center panels), which is calculated based on the monthly averaged nighttime surface [NO_3] map (left panels) and monthly averaged nighttime surface reactive organic gases ([ROG]) (right panels), which is a sum of isoprene (ISOP), internal (OLI) and external (OLT) olefins.

ACPD
12, 5189–5223, 2012

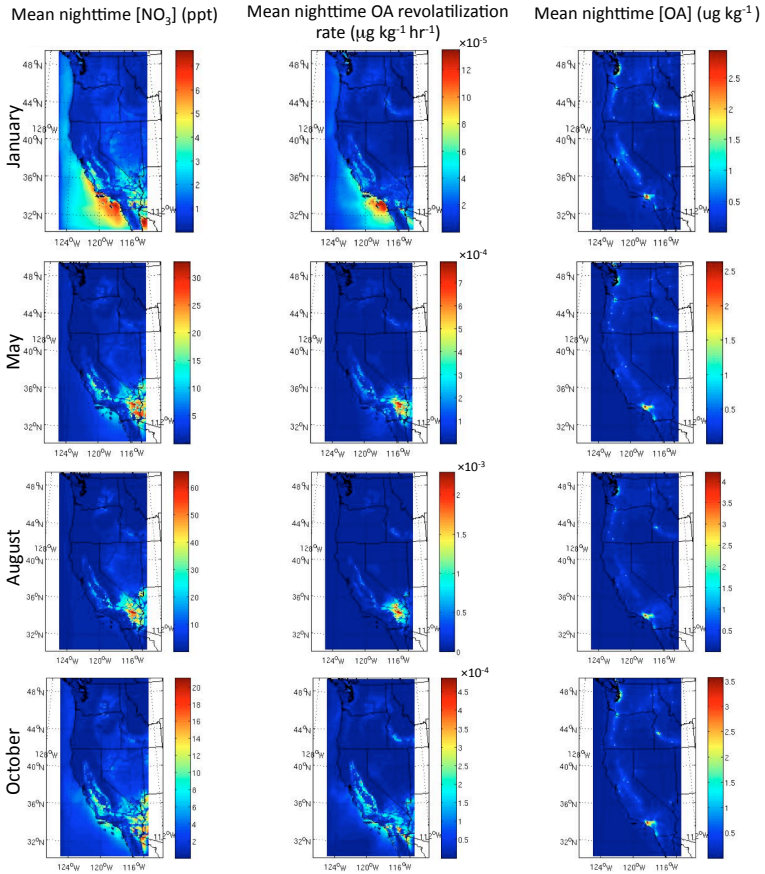

Fig. 5. Seasonal pattern of NO_3-initiated OA revolatilization (sink) rate (center panels), which is calculated based on the monthly averaged nighttime surface [NO_3] map (left panels) and monthly averaged nighttime [OA] (right panels).

ACPD
12, 5189–5223, 2012

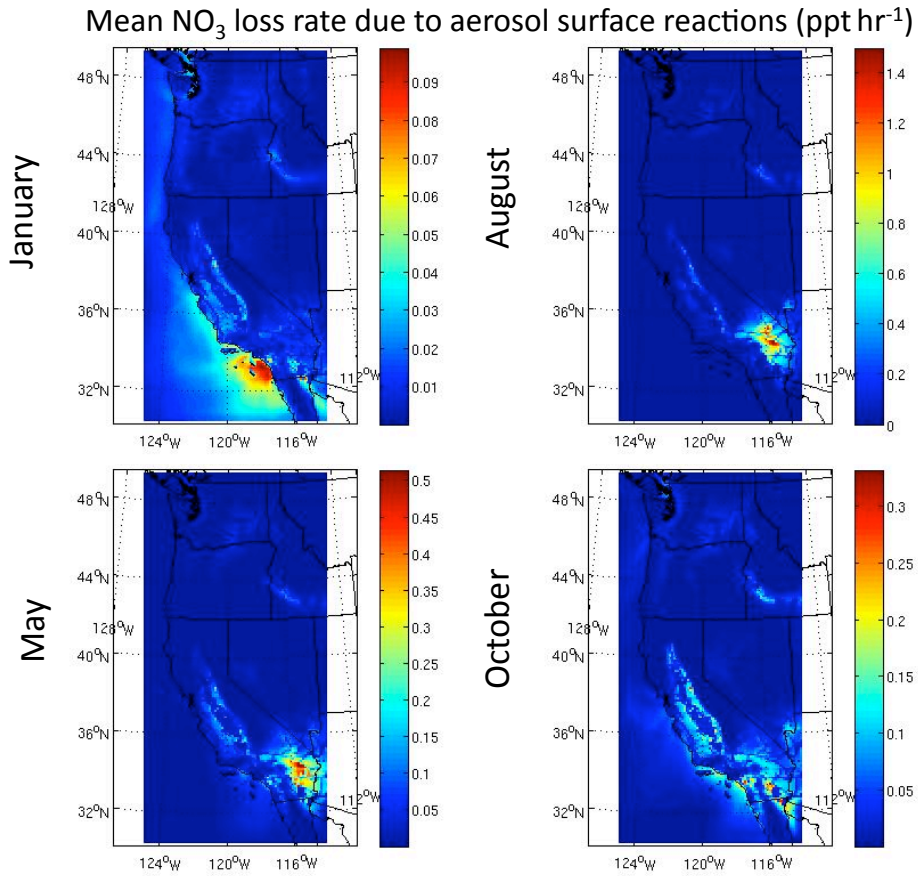

Fig. 6. Seasonal pattern of NO_3 loss rate as a result of heterogeneous reactions on OA surfaces.

ACPD
12, 5189–5223, 2012

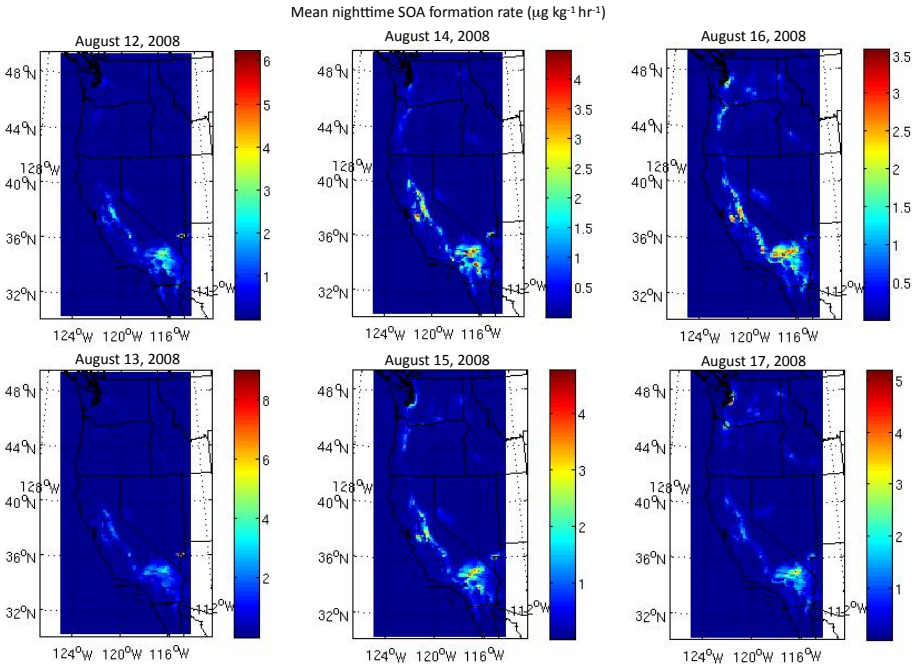

Fig. 7. Several individual nights' averages of the NO_3-initiated SOA source, showing spatial and magnitude variability for the Western United States domain.

ACPD
12, 5189–5223, 2012

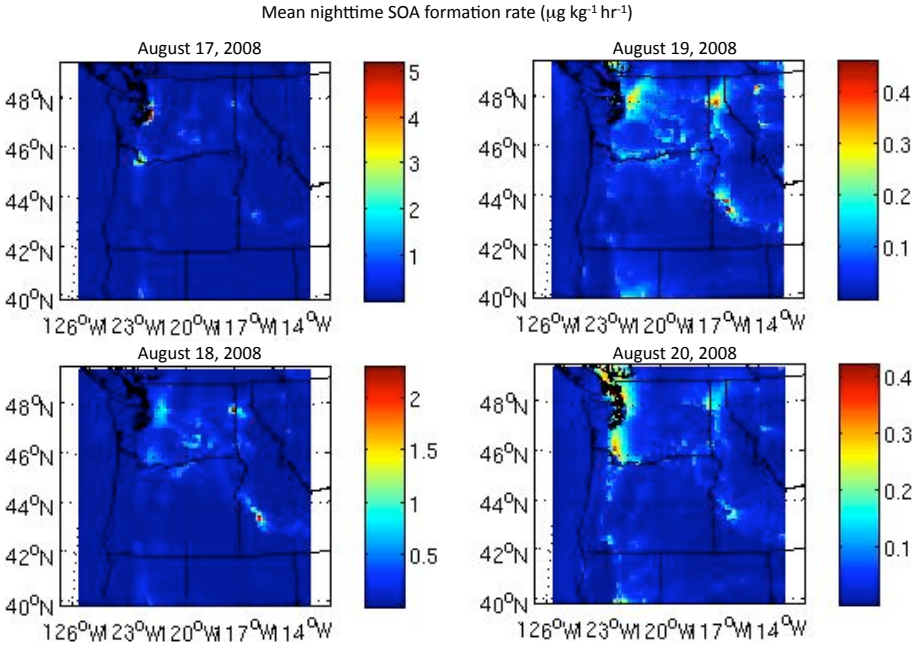

Fig. 8. Zoom-in on the Pacific Northwest to demonstrate spatial and temporal variability of NO_3-initiated SOA source in this lower-NO_3-concentration region.

ACPD
12, 5189–5223, 2012

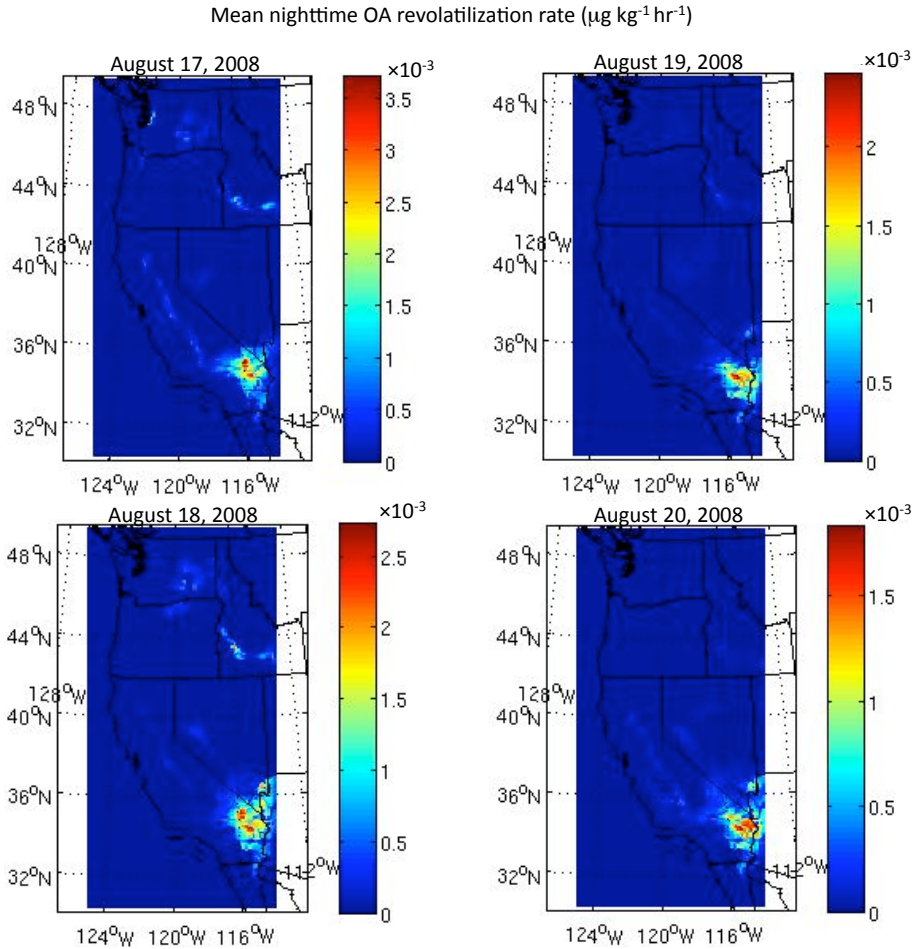

Fig. 9. Several individual night's averages of the NO_3-initiated OA loss, showing spatial and magnitude variability for the Western United States domain.

ACPD
12, 5189–5223, 2012

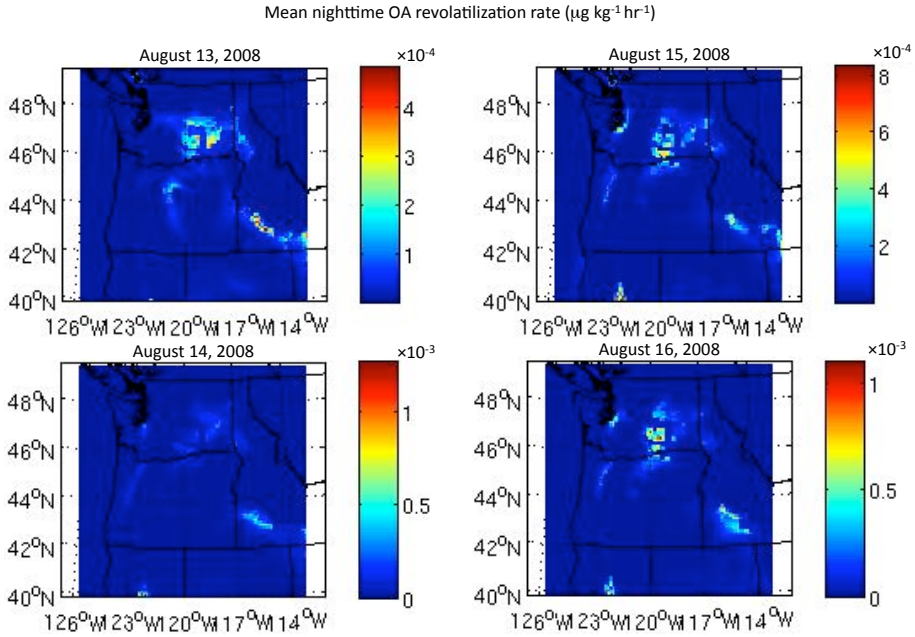

Fig. 10. Zoom-in on the Pacific Northwest to demonstrate spatial and temporal variability of NO_3 OA loss in this lower-NO_3-concentration region.

ACPD
12, 5189–5223, 2012